ORIGINAL PAPER

Fluorescence biosensing micropatterned surfaces based on immobilized human acetylcholinesterase

**Manuela Bartolini · Marina Naldi · Dan V. Nicolau ·
Falco C. M. J. M. van Delft · Jeroen van Zijl ·
Jaap Snijder · Eric F. C. van den Heuvel ·
Emile P. Naburgh · Natalia Calonghi ·
Vincenza Andrisano**

Abstract Human acetylcholinesterase (AChE) is a widely studied target enzyme in drug discovery for Alzheimer's disease (AD). In this paper we report evaluation of the optimum structure and chemistry of the supporting material for a new AChE-based fluorescence sensing surface. To achieve this objective, multilayered silicon wafers with spatially controlled geometry and chemical diversity were fabricated. Specifically, silicon wafers with silicon oxide patterns (SiO$_2$/Si wafers), platinum-coated silicon wafers with SiO$_2$ patterns (SiO$_2$/Pt/Ti/Si wafers), and Pt-coated wafers coated with different thicknesses of TiO$_2$ and SiO$_2$ (SiO$_2$/TiO$_2$/Pt/Ti/Si wafers) were labelled with the fluorescent conjugation agent HiLyte Fluor 555. Selection of a suitable material and the optimum pattern thickness required to maximize the fluorescence signal and maintain chemical stability was performed by confocal laser-scanning microscopy (CLSM). Results showed that the highest signal-to-background ratio was always obtained on wafers with 100 nm thick SiO$_2$ features. Hence, these wafers were selected for covalent binding of human AChE. Batch-wise kinetic studies revealed that enzyme activity was retained after immobilization. Combined use of atomic-force microscopy and CLSM revealed that AChE was homogeneously and selectively distributed on the SiO$_2$ microstructures at a suitable distance from the reflective surface. In the optimum design, efficient fluorescence emission was obtained from the AChE-based biosensing surface after labelling with propidium, a selective fluorescent probe of the peripheral binding site of AChE.

M. Bartolini · M. Naldi · V. Andrisano (✉)
Department of Pharmaceutical Sciences, University of Bologna,
40126 Bologna, Italy
e-mail: vincenza.andrisano@unibo.it

D. V. Nicolau
Department of Electrical Engineering & Electronics,
University of Liverpool,
Liverpool L69 3GJ, UK

F. C. M. J. M. van Delft · J. van Zijl · J. Snijder ·
E. F. C. van den Heuvel
Technology Labs., Philips Innovation Services,
High Tech Campus 4,
5656 AE Eindhoven, The Netherlands

E. P. Naburgh
Q&R Surface Analysis, Philips Innovation Services,
High Tech Campus 4,
5656 AE Eindhoven, The Netherlands

N. Calonghi
Department of Biochemistry, University of Bologna,
40126 Bologna, Italy

Introduction

Protein immobilization on solid surfaces is the initial step in the development of new sensing devices that can be integrated into protein chip microarrays or enzyme reactors [1]. In the current search for speed and automation, sensing surfaces which operate with immobilised biomolecules have found a broad range of applications in the life sciences [2].

In particular, the drug-discovery process, in which a large number of compounds must be screened for affinity for a specific target, will greatly benefit from miniaturization and automation of screening systems. To achieve this, fabrication and derivatisation techniques have enabled the development of new engineered surfaces, which can be interfaced with different detection methods [1, 2]. Because of their small area, sensing surfaces containing immobilized proteins could enable higher screening speeds and lower consumption of chemicals and analytes.

Acetylcholinesterase (AChE), the enzyme involved in the degradation of the cholinergic neurotransmitter acetylcholine in the brain and peripheral nervous system, is the primary target of drugs for cholinergic pathway-related human diseases such as Alzheimer's disease (AD). AD is the most frequent form of dementia and affects nearly 36 million people worldwide [3]. Indeed, in recent decades, reversible AChE inhibitors have been clinically used for treatment of the symptoms of AD [4]. Furthermore, in addition to action of AChE on cholinergic synapses, it has been hypothesised that AChE's peripheral binding site (PAS) promotes the deposition of the neurotoxic β-amyloid peptide (Aβ) [5–7]. Therefore, because of this activity, new AChE inhibitors, able to prevent the interaction between AChE's PAS and Aβ, are under intense investigation [8]. Several AChE-based enzyme reactors have been developed for automated and rapid screening of inhibitors at the catalytic binding site (CAS) [9, 10]. Most previous investigations have been performed by using chromatographic materials as solid supports [11–13]. However, the chromatographic approach has limitations to miniaturization and it is not suitable for optical methods. Moreover, immobilization on to a chromatographic support does not generally enable direct visualization of the interaction of a fluorescent probe with the target enzyme, as is required for identification of PAS binding agents. To overcome this problem, an AChE bio-chip built on a suitable supporting material can be used instead. The supporting material selected should facilitate detection of binding by use of imaging techniques [1].

Silicon-based materials and surfaces are commonly used in association with microscopy techniques and have been proved to be suitable for the development of several DNA and protein-based bio-chips [14]. However, when a silicon surface or, in general, a reflective surface is used for fluorescence-based experiments, the fluorescence interference contrast (FLIC) phenomenon, either constructive or destructive, must be taken into account. Because of the FLIC phenomenon, the fluorescence emission intensity is enhanced or suppressed as a consequence of the proximity of the fluorophore to the reflective surface [15, 16]. Consequently, the fluorescence signal depends on the surface architecture and, specifically, on the distance between the fluorophore and the reflective surface. Thus, in the development of a new AChE-based sensing surface, the optimum surface chemistry and

structure should not only enable stable immobilization of AChE without suppressing its catalytic activity, but also enhance the output signal related to specific fluorescent binders and ensure stability over time. To address these issues, in this work, different micropatterned wafers with a reflective layer (either platinum or silicon) and SiO₂ pillars, lines, and holes were fabricated and tested. The final objective was selection of a biomolecular-optimum surface with improved sensitivity because of reduction of unwanted side phenomena, for example fluorescence quenching or protein denaturation related to proximity to a metal surface.

Materials and methods

Chemicals and proteins

(S)-Acetylthiocholine iodide, 5,5′-dithio-bis(2-nitrobenzoic acid) (DTNB; Ellman's reagent), glutaraldehyde 70 % aqueous solution, propidium iodide (3,8-diamino-5,3′-diethylmethylamino-n-propyl-6-phenylphenanthridium), (3-aminopropyl) triethoxysilane (APTES), magnesium chloride, Tris(hydroxymethyl)aminomethane, hydrochloric acid (37 %), dipotassium hydrogen phosphate anhydrous, aqueous ammonia solution (28 %), methanol of HPLC grade, glycerol, and recombinant human acetylcholinesterase (hAChE, E.C. 3.1.1.7) lyophilized powder were purchased from Sigma Chemical (Milan, Italy). Hydrogen peroxide (30 %) was from Fluka (Milan Italy) and potassium dihydrogen phosphate of analysis quality was from Carlo Erba Reagenti (Milan, Italy).

Hellmanex cleaning solution was purchased from Hellma (Germany). AnaTag Hylite Fluor 555 microscale protein labelling kit (Abs/Em=550/566 nm) was from AnaSpec (USA). Purified water from a TKA ROS 300 system was used to prepare buffers and solutions. Bi-distilled water and buffer solutions were filtered through 0.22-μm nitrocellulose membrane filters (Millipore) before use.

Fabrication of silicon wafers

Silicon wafers (diameter 4 in) were coated with different layer stacks in a Veeco Nexus 800 sputter deposition tool (Table S1 in Electronic Supplementary Material). All wafers were briefly directly sputter-cleaned in situ before the first deposition. Parts of the wafers were sputter coated with 100 nm Pt after deposition of a 10 nm thick Ti adhesion layer. On both Pt-coated and uncoated silicon wafers, different thicknesses of quartz were sputter deposited. Pt-coated wafers coated with different thicknesses of TiO₂, then with different thicknesses of quartz (SiO₂/TiO₂/Pt/Ti/Si wafer) were fabricated so the total (SiO₂+TiO₂) layer thickness was 100 nm. Next, an HPR504 resist layer 1.5 μm thick was spin coated, prebaked, and exposed in an ASML i-

line stepper using a standard lines-and-spaces test reticle. After development of the resist, these patterns were used as mask in a CHF$_3$ plasma for etching the quartz and TiO$_2$ down to the Pt layer or Si (with a 10 % over-etch time). This was followed by brief use of a high-pressure oxygen–nitrogen plasma to "open up" the resist residues (removal of "Teflon"-type top layer) for the subsequent wet-chemical resist removal. Finally, the pattern height was measured by use of an α-step profilometer.

Derivatisation and labelling of silicon wafers

W01–05

Silicon wafers #01 to #05 were cleaned by use of the procedure described by Han et al. [17] In brief, the wafers were sonicated in ethanol (10 min), immersed in Hellmanex aqueous solution (2 %) for 10 min, and rinsed and sonicated in bi-distilled water (5 min). The wafers were then rinsed with methanol and immersed for 30 min in HCl (37 %)–MeOH (50:50, *v/v*) at room temperature (RT). Silanization of the oxide surfaces was performed at 50 °C for 2 h by immersing the wafers in 5–10 mL (3-aminopropyl)triethoxysilane (APTES) in ethanol (10 %*w/v*). After rinsing with ethanol, the wafers were immersed in acetic acid (1 mmol L^{-1}) for 15 min, rinsed with bi-distilled water and EtOH, and dried. Next, 80 μL HyLite Fluor solution (34.5 μmol L^{-1}) was added to each wafer and kept at RT for 30 min. Wafers were rinsed with water and stored in glycerol–H$_2$O 50:50 (*v/v*) at 4 °C.

W06–11

Wafers #06 to #11 were cleaned by the standard RCA-1 + RCA-2 procedure which entails use of a basic cleaning solution (H$_2$O–H$_2$O$_2$–NH$_3$(aq) 5:1:1) at 70 °C (5 min) followed by treatment with an acid cleaning solution (H$_2$O–H$_2$O$_2$–HCl 6:1:1) at 70 °C (5 min). Next, the wafers were rinsed with bi-distilled water and immersed for 2 h in ethanol–4.25 mol L^{-1} acetic acid–APTES (87:3:10*v/v*) at RT, rinsed with bi-distilled water and EtOH, dried, and labelled with HyLite Fluor 555 by use of the procedure described for W01–05.

W12–16

After cleaning, wafers #12 to #16 were immersed for 5 min in HCl (37 %)–MeOH (25:75*v/v*) at RT then and rinsed with EtOH. Silanization was performed at 50 °C for 2 h by immersing the wafers in 5–10 mL APTES solution (10 % *w/v* in ethanol). The wafers were then rinsed with ethanol and immersed in acetic acid (1 mmol L^{-1}) for 15 min, rinsed

with bi-distilled water and EtOH, dried, and labelled by use of the procedure described for W01–05.

Covalent linkage of hAChE

A freshly aminosilanized W05 wafer was immersed in 10 mL 12.5 % glutaraldehyde solution in phosphate buffer (10 mmol L^{-1}, pH 8.0) and kept at 32±2 °C for 4 h, in the dark. The wafer was then washed with phosphate buffer (10 mmol L^{-1}, pH 8.0). Recombinant hAChE (99.4 units; 120 μL) was applied to the wafer surface and left to react overnight in the dark. After this time, the residual activity was determined by Ellman's method [18]. The wafer was washed with phosphate buffer (10 mmol L^{-1}, pH 8.0) and stirred for 3 h with 0.2 mol L^{-1} monoethanolamine solution in phosphate buffer (10 mmol L^{-1}, pH 8.5) to inactivate residual primary amino groups. Finally the AChE-Si wafer was washed with phosphate buffer (10 mmol L^{-1}, pH 7.4) and stored in the same buffer at 4 °C until use.

Colorimetric determination of AChE activity and kinetic data

The activity of unbound and covalently bound AChE was assessed by Ellman's method [18] (Electronic Supplementary Material).

Kinetic data for AChE–Si wafer were determined by evaluating enzyme activity (μmoles of product formed per min) at increasing substrate concentration (0.35–5.61 mmol L^{-1}). K_m and v_{max} values were derived (GraphPad Prism; GraphPad Software, USA) from the obtained Michaelis–Menten plot and the immobilized active units were calculated.

Reversible labelling of immobilized hAChE by propidium

Propidium iodide solution (100 μmol L^{-1} in Tris HCl buffer 1.0 mmol L^{-1}, pH 8.0; 100 μL) was applied to the AChE-Si wafer and incubated for 30 min at RT, in the dark. Next, the AChE-Si wafer was washed with Tris HCl buffer (1.0 mmol L^{-1}, pH 8.0) and the fluorescence distribution was qualitatively evaluated by CLSM.

Confocal laser-scanning microscopy (CLSM)

Images were acquired by sequential laser excitation at 543 nm and capture with a Nikon C1s confocal laser-scanning microscope equipped with a Nikon PlanApo 100X, oil immersion lens. For spectral imaging, wafers were embedded in water–glycerol (50:50). For confocal spectral analysis, the sample was excited at 543 nm with an argon laser, and fluorescence was detected in spectral mode in the range 560–670 nm at 5 nm resolution. At least three spots

on a fluorescently labelled area were measured, and the spectra were averaged and corrected for background fluorescence by subtracting fluorescence emission spectra detected at a pattern-free region on the same sample.

Atomic force microscopy (AFM)

AFM analysis was performed with a NT-MDT atomic force microscope (Smena Nova, Moscow, Russia). Pattern morphological investigations were conducted in semi-contact mode, in air, under the following conditions: scan rate 0.5 Hz, NSG11 golden silicon probes (NT-MDT) with tip apex radius of 10 nm, resonant frequency range of AFM cantilever 115–325 Hz, and number of pixels 512×512. The images were processed off-line with Gwiddion 2.17 software. For roughness studies, images were processed off-line with Image Analysis 2.2.0 software by applying a flattening algorithm to remove the background slope. Line analysis (5 μm) was then performed and the average roughness, R_a, ($n=20$) both on the top and the bottom of the silicon oxide pattern, was derived.

Scanning Auger microscopy and scanning electron microscopy

Scanning Auger microscopy (SAM) imaging, Auger spectral measurements, and scanning electron microscopy (SEM) imaging were performed with a Physical Electronics PHI 670sxi nanoscope Scanning Auger microscope with primary beam settings of 5 kV and 20 nA. The Auger measurements were performed with a energy resolution of 1 or 2 eV per step. Stylus measurements were performed with a Veeco Dektak 6 M profilometer equipped with a stylus of 12.5 μm radius. The scanned length was 1000 μm.

Results and discussion

Reflective surfaces may have the advantage of higher output signals when fluorescence detection is used. In this work, two different reflective surfaces (platinum and silicon, with micrometer-sized mono-layer or bi-layer silicon dioxide structures on top) were selected for investigation. In particular, silicon wafers (diameter 4 in) with quartz patterns (SiO_2/Si wafers, W01–05) platinum-coated silicon wafers with quartz patterns ($SiO_2/Pt/Ti/Si$ wafers, W06–11), and Pt-coated wafers coated with different thicknesses of TiO_2, then with different thicknesses of quartz ($SiO_2/TiO_2/Pt/Ti/Si$ wafers, W12–16) were manufactured and investigated (Table 1).

Optimization of surface derivatisation

Initial studies were performed to optimize the derivatisation procedure with the double objective of:

1. achieving homogeneous derivatisation of silicon oxide structures without damaging the silicon oxide geometry; and
2. selecting the optimum chemistry and structure to achieve a high fluorescence signal.
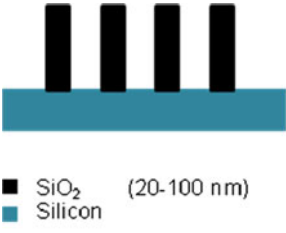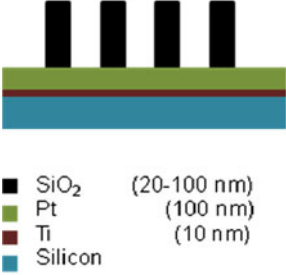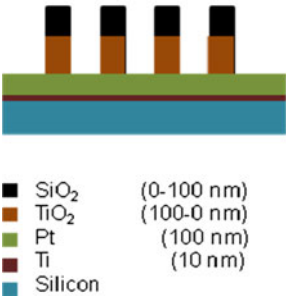
In the optimization phase, HiLyte Fluor 555 was used as fluorescent conjugation agent to visualize the silicon oxide pillars, lines, and holes (Fig. S1 in Electronic Supplementary Material) and to investigate the FLIC effects. On the basis of FLIC theory [16, 19], the observed fluorescence signal is modulated by the distance of the fluorophore from the reflective surface. Therefore, the fluorescence output may be enhanced or suppressed by varying this distance. Consequently, the effect of the distance between the fluorophore and the metal surface was investigated by fabricating wafers with the top surface of the SiO_2 pattern elevated 20–100 nm above the reflective surface, and the effect of type of metal was studied by fabricating silicon wafers coated with two different reflective surfaces (silicon or platinum) (Table 1).

The wafers were first cleaned and then amino-silanized with APTES under mild conditions [17] to obtain H_2N wafers (Fig. S2 in Electronic Supplementary Material). To avoid stability problems related to enzyme denaturation and to reduce optimization costs, a fluorescent labelling agent (HiLyte Fluor 555) was used in the optimization phase. The conjugation agent was selected on the basis of similarity of its optical properties (maximum Ex/Em wavelength = 550/566 nm) with those of propidium iodide, a fluorescent AChE binder [20], which was used in further experiments. Confocal fluorescence micrographs showed that the distribution of the fluorescent agent perfectly matched the initial SiO_2 patterns, both on the platinum coated (W06–11) and non-platinum coated (W01-05) silicon wafers (Fig. 1), irrespective of the height of the SiO_2 patterns.

To quantitatively measure the dependence of fluorescence emission intensity (FI) on silicon dioxide thickness, confocal spectral analysis ($\lambda_{exc}=543$ nm) were performed by recording emission spectra in the range 560–670 nm. Data for both the SiO_2/Si (W01–05) and $SiO_2/Pt/Ti/Si$ (W06–11) wafers showed that FI increased when the distance between the fluorophore and the reflective surface increased (Fig. 2).

The signal-to-background ratio was highest for wafers with 100 nm-high features (W05 and W11). Among the bare silicon wafers, the fluorescence intensity of W05 (100 nm-thick SiO_2 pattern) was approximately 4.4 times higher than that obtained with W01 (20 nm-thick pattern).

Table 1 Properties of bilayered and multilayered silicon wafers (diameter 4 in). Layer thickness and the wafer identification code are reported

Wafer nr.	Stack:	Ti d(nm)	Pt d(nm)	TiO2 d(nm)	SiO$_2$ d(nm)	RIEed up till	Measured pattern(nm)
01		0	0	0	20	Si	24
02		0	0	0	40	Si	46
03		0	0	0	60	Si	67
04		0	0	0	80	Si	82
05		0	0	0	100	Si	104
06		10	100	0	0	-	1500
07		10	100	0	20	Pt	21
08		10	100	0	40	Pt	42
09		10	100	0	60	Pt	61
10		10	100	0	80	Pt	81
11		10	100	0	100	Pt	101
12		10	100	100	0	-	1500
13		10	100	80	20	Pt	100
14		10	100	60	40	Pt	104
15		10	100	40	60	Pt	104
16		10	100	20	80	Pt	103

Legend (top schematic):
- SiO$_2$ (20-100 nm)
- Silicon

Legend (middle schematic):
- SiO$_2$ (20-100 nm)
- Pt (100 nm)
- Ti (10 nm)
- Silicon

Legend (bottom schematic):
- SiO$_2$ (0-100 nm)
- TiO$_2$ (100-0 nm)
- Pt (100 nm)
- Ti (10 nm)
- Silicon

Next, the effect of the metal surface on the FI was evaluated by comparing uncoated and Pt-coated silicon wafers with SiO$_2$ patterns of identical height. The maximum FI of W11 was 2.7±0.2 times higher than that obtained with W05. This is in reasonable agreement with the perpendicular reflection coefficients (R) as calculated from the n and k refractive index values for the SiO$_2$/Pt and SiO$_2$/Si interfaces; these values are $R=0.53$ and 0.23 at 543 nm, and $R=0.59$ and 0.21 at 632 nm [21]. Therefore, the theoretical fluorescence enhancement factor for the platinum coating on silicon is 2.3 at 543 nm and 2.8 at 632 nm.

On the basis of the results presented, the SiO$_2$/Pt/Ti/Si wafer with the 100-nm thick SiO$_2$ pattern (W11) was preferred, because it results in the highest fluorescence signal enhancement. However, the SiO$_2$/Pt/Ti/Si wafers proved to be less chemically robust and were frequently damaged during derivatisation, e.g. detachment of SiO$_2$ patterns from the platinum layer. This may be because the SiO$_2$–Pt bond is weaker than the Pt–Pt and Si–O bonds, which makes the SiO$_2$/Pt/Ti/Si wafers less suitable for biochemical applications, because of their instability in aqueous solutions. To overcome the instability problems during derivatisation, the

Fig. 1 Representative confocal scanning micrographs (*top*) and AFM images (*bottom*) of lines, pillars, and holes. Micrographs were acquired after labelling SiO_2 patterns with a red-emitting fluorescent probe, λ_{exc}=543 nm. Magnification = 100×, gain ×2. AFM analysis was performed in semi-contact mode and the resulting images were processed off-line to remove the background slope. *Scale bars* are 20 μm
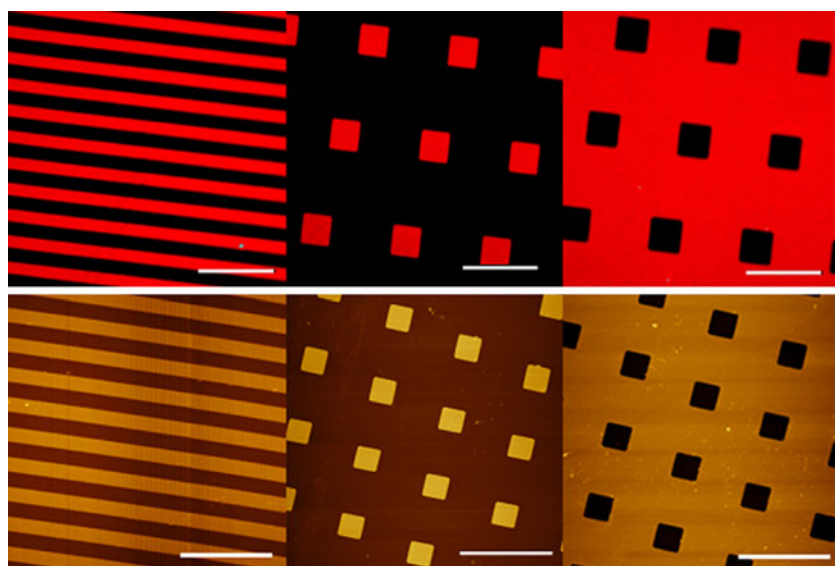
derivatisation procedure was modified to reduce the time in strongly acidic conditions while maintaining good derivatisation yield. Under the optimized conditions, no damage to the Pt-coated wafers (W06–W11) was observed during the derivatisation and labelling steps. However their stability under storage conditions was still quite limited (Fig. S3 in Electronic Supplementary Material). Therefore, in an attempt to produce wafers with greater stability, a new series of multi-layered wafers was fabricated by introducing a TiO_2 layer (from 20 to 80 nm high) as an adhesion layer between the Pt surface and the SiO_2 structures (W12–W16, Table 1). In this new series the total height of the pattern (given by the TiO_2 layer + the SiO_2 layer) was kept constant at 100 nm. Structures with a TiO_{2-x} layer were more stable, as expected from the so-called strong metal support interaction (SMSI) effects [22]. From an optical perspective, the thickness of the TiO_2 layer relative to that of the SiO_2 layer
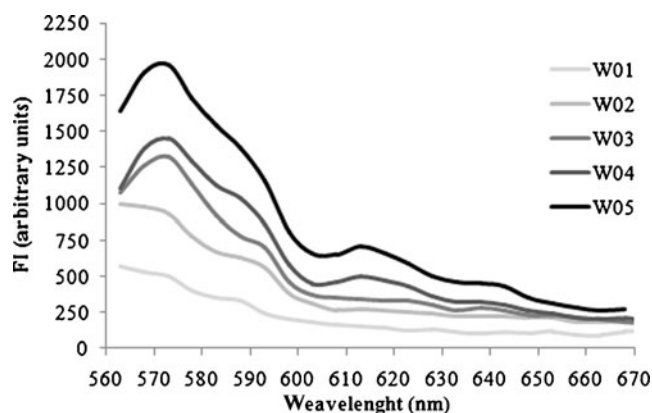

Fig. 2 Confocal spectral analysis of labelled W01–05 wafers (λ_{exc}= 543 nm). Each emission spectrum is the average of spectra from three different spots on a homogeneously labelled area, corrected for the background fluorescence detected at a pattern-free region on the same sample

affected the fluorescence interference. The behaviour of the fluorescence of the $SiO_2/TiO_{2-x}/Pt/Ti/Si$ wafers was very complicated, probably because of variation of the oxygen content along the TiO_{2-x} layer when going from the SiO_2 to the Pt interfaces. This variation could result in a variable refractive index and variable reflective properties. Among the TiO_{2-x} series, sample W16 (containing a 20-nm TiO_2 layer) gave the highest fluorescence signal, but its fluorescence emission intensity was much lower than those of W11 (−78 %) and W05 (−40 %).

It should be noted that for SiO_2/Si wafers, this adhesion problem is not present, because silicon has always a native oxide surface layer, that has a good lattice match and good adhesion to Si. This was experimentally confirmed by long-term studies on fluorescently labelled W05. Indeed, after one year no morphological alterations were observed for HiLyte Fluor 555-labelled W05 (CLSM analysis), and the residual FI was 49.5 %. In contrast, widespread detachment of the SiO_2 features from the platinum surface was observed for the corresponding platinum-coated wafer W11 after storage for only 21 days (Fig. S3 in Electronic Supplementary Material). Under the same conditions, W16 (with a 20 nm TiO_2 layer) was more stable. However, CLSM analysis revealed surface inhomogeneity, indicative of initial alteration of the morphology the wafer. Overall, the order of descending stability was W05 > W16 > W11.

On the basis of these results, the uncoated silicon wafer with the 100-nm-thick SiO_2 pattern was selected for immobilization of human AChE.

Covalent binding of human AChE

Because the proximity to a flat surface had previously been reported to alter the biological behaviour of human AChE
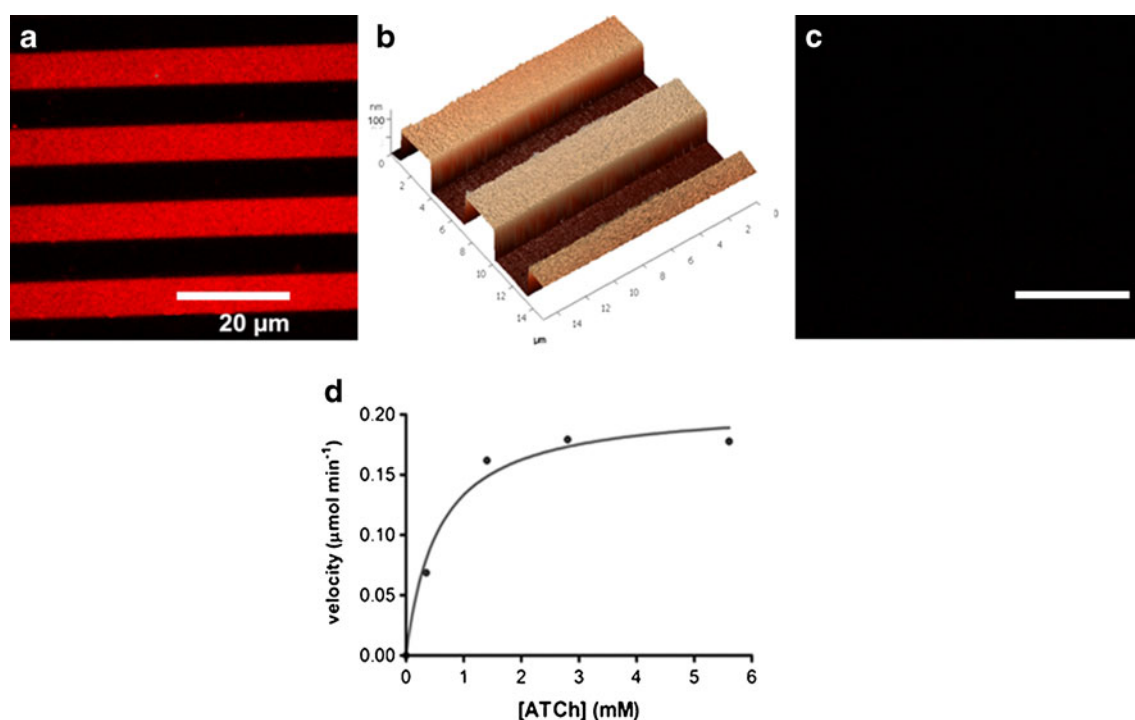
Fig. 3 Qualitative and quantitative analysis of immobilized AChE. (**a**) Confocal scanning micrograph of propidium-labelled AChE-W05 (*red areas*); (**b**) 3D AFM image of W05 surface showing SiO$_2$ lines on a flat silicon surface; (**c**) no fluorescence emission was detected when aminosilanized surfaces without any AChE were treated with propidium; (**d**) Michaelis–Menten plot for AChE-W05. *ATCh*, acetylthiocholine (substrate)

[11], a chain spacer was introduced by reacting the primary amino groups of H$_2$N-W05 with 12.5 % glutaraldehyde solution (Fig. S2 in Electronic Supplementary Material). Indeed, introduction of a five-carbon spacer chain had previously been shown to limit alteration of the kinetics of the enzyme [11]. Stable hAChE immobilization was then achieved by covalent linkage between the enzyme primary amino groups of the lysine lateral chain and the aldehydic residues on the derivatised W05.

The retained enzyme activity after linkage was measured by Ellman's assay [18] and the specific distribution of the enzyme was evaluated by CLSM, using propidium iodide as selective fluorescent marker. Propidium binds with high affinity to the PAS of AChE [23], with tenfold enhancement of its fluorescence [24].

Apart from being an ideal fluorescent probe for morphological analysis of the hAChE distribution, propidium was also selected because of its use in displacement studies for PAS binders. Indeed, evaluation of the ability of an AChE inhibitor to interact with the PAS is an important aspect of drug discovery, because AChE is also a potent amyloid fibrillogenesis-promoting agent [5–7]. It has been suggested this promoting action is related to the interaction of amyloid peptides with the PAS [5, 7]. Propidium displacement experiments can be conducted to evaluate whether new chemical entities bind to PAS and, consequently, affect amyloid aggregation and disease progression.

Analysis by CLSM of propidium labelled AChE-W05 showed that the enzyme distribution perfectly matched the SiO$_2$ features (Fig. 3a, b). To exclude false positive staining,

Table 2 Average roughness of silicon wafer W05 (100-nm-thick silicon oxide pillars, holes, and lines on a silicon flat surface), $n=20$. Each line analysis was performed on a 5 μm length. Measurement was perpendicular to the scanning direction

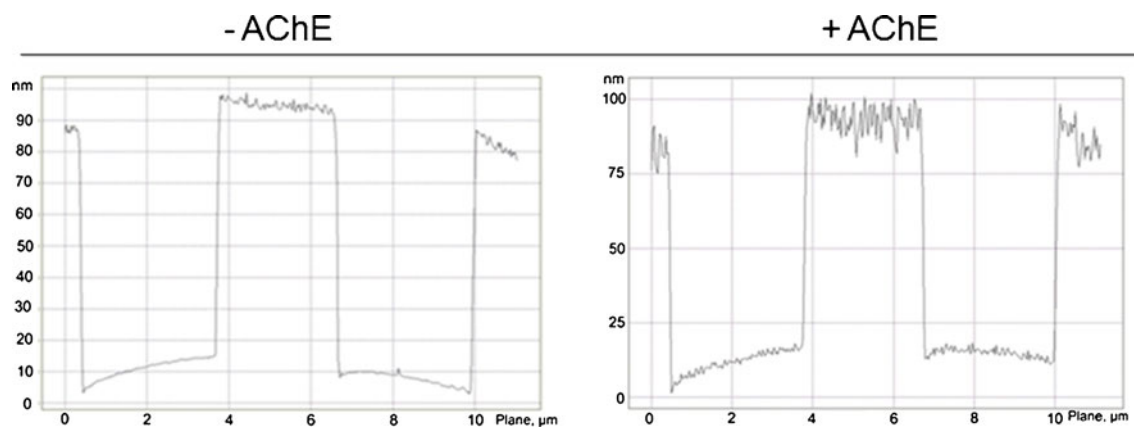|	R_a top ($\pm$ SD)	R_a bottom ($\pm$ SD)
Untreated wafer (reference)	1.41±0.17	0.37±0.03
Wafer after APTES derivatisation	1.51±0.24	0.86±0.20
R_a difference	+0.10	+0.49
Wafer after covalent linkage of AChE	6.10±0.50	1.33±0.14
R_a difference compared with untreated wafer	+4.69	+0.96
R_a difference compared with APTES-treated wafer	+4.59	+0.47

Fig. 4 Average roughness analysis by AFM. 5 μm line analyses for W05 before enzyme immobilization (*left panel*) and after enzyme covalent immobilization (*right panel*) are shown

an aminosilanized wafer (H₂N-W05) was treated with a solution of propidium iodide. The absence of any fluorescence signal (Fig. 3c) enabled definitive exclusion of the possibility of non-specific adsorption of propidium on enzyme-free surfaces.

Another important issue to be checked is false negative staining related to complete suppression of the fluorescence signal at the metal surface. This aspect is important to further confirm that the enzyme distribution was mainly confined to the top of the SiO_2 features. To check this, the average roughness (R_a) of the top and bottom of the pillars and lines was determined by AFM (line analysis).

It is conceivable that surface roughness is increased as a consequence of enzyme binding. In agreement with our hypothesis, the data in Table 2 show that R_a at the top of derivatised SiO_2 features increased significantly after covalent linkage of hAChE (+4.59) whereas variation of R_a of the silicon surface bottom areas was much lower (+0.47) (Fig. 4). It should be noted that after cleaning and aminosilanization only small increases of the R_a values of the top and bottom areas were observed (+0.10 and +0.49, respectively). Therefore, the final increase of the roughness on the top of the structures cannot be ascribed to selective etching of the oxide structures during the cleaning

procedures, but suggests a selective confinement of hAChE to the top of the structures.

To investigate on the original wafer whether the chemical composition on the top of the structures was different from that in the region between the structures, and whether this also was valid for the sample after cleaning, APTES treatment, and AChE linkage, scanning Auger microscopy–scanning electron microscopy (SAM-SEM) measurements were performed on W05 before and after enzyme immobilization. As expected, on the top surface of untreated W05 the Si-to-O ratio was 1:2. On the other hand, higher C and O signals from the etched zones (and occasional above-threshold traces of F) are indicative of partly oxidized Teflon type residues, because of the CHF_3 plasma treatment followed by brief O_2 plasma oxidation (step 14 in Table S1 in Electronic Supplementary Material), which indicates that the fabrication procedure generated a chemical contrast between the top of the structures and the bottom areas (Table 3). The lower Si Auger signal (at 93 eV) in the etched region is because of its surface sensitivity; despite the fact that a Si surface should have a higher Si signal than an SiO_2 surface, the adsorbed residues in the etched region are very effective in quenching the signal.

The results after APTES and AChE treatment are more difficult to interpret. It may be noted that, both on the SiO_2

Table 3 Combined profilometer, SEM, and SAM analyses

Sample	Profilometer position	SEM appearance	SAM (apparent atomic %) uncorrected for surface sensitivity				
			C	N	O	Si	F
W05-untreated	Top SiO₂	Dark	10±1	<1	60±1	30±1	<0.2
	Etched area	Bright	16±2	<1	63±2	20±2	0.2±0.2
W05-AChE	Top SiO₂	Bright	24±2	2.1±0.4	50±2	24±1	<0.2
	Etched area	Dark	35±2	2.3±0.5	32±3	30±2	<0.2

top surfaces and in the etched areas, the C signal is increased and N is detected, indicative of derivatisation of the Si/SiO$_2$ layer in both regions. Indeed the increase in the N content may be derived from both the APTES and/or the enzyme. The Si-to-O ratio on the SiO$_2$ top surface is 1:2, although both signals are slightly quenched by the adsorbates. From the reduction of the F levels, it also seems that the chemical contrast because of Teflon-type residues on the reference sample may have largely disappeared after cleaning and/or derivatisation. On the other hand, the Si-to-O ratio between the structures is now close to unity; this might indicate that the native oxide also is (completely or partly) removed, restoring (to some extent) an Si/SiO$_2$ chemical contrast between the bottom and the top of the structures. It should be noted that (part of) the oxygen signal may arise from the attached APTES and/or AChE.

Overall, because of the chemical contrast between the top of the structures and the etched areas of the W05 wafer, surface derivatisation is likely to have occurred to different extents on the top and the bottom areas. This may explain the results from the propidium-based investigation and from roughness analysis, both of which support prevalent confinement of the enzyme to the top of the silicon oxide architectures.

To the best of our knowledge this is the first study performed to develop a microstructured hAChE-based biosensing surface for fluorescence displacement studies. Whereas a few previous investigations on AChE-based nano-structured surfaces have been reported, the purpose of these studies was, usually, measurement of intrinsic AChE activity and/or inhibition [25–27], particularly for pesticide detection.

Activity of immobilized hAChE

Evaluation of the amount of active enzyme covalently bound by the solid support is a key step in verification that the active structure of the enzyme is maintained. A slightly modified Ellman's assay [18] adapted to evaluation of covalently bound hAChE [11, 12, 28] was used. Comparison of the activity of the enzyme before and after immobilization enabled evaluation of the yield of immobilization, which was 46 %. Moreover, from the Michaelis–Menten plot (Fig. 3d), kinetic data for the covalently immobilized hAChE were determined (v_{max}=0.21 μmol min^{-1} and K_m=0.56 mmol L^{-1}). The amount of immobilized active enzyme is 0.21 international units (IU) per square centimetre, corresponding to 12.6 μg enzyme.

Conclusions and perspectives

In this study bilayered and multilayered micro-patterned wafers were fabricated and analysed as optimum support material for the development of a new sensing surface containing immobilised hAChE for fluorescence-based experiments. Irrespective of the metal layer at the bottom of the SiO$_2$ pattern, wafers with 100 nm thick SiO$_2$ features resulted in the highest signal-to-background ratio, because of the FLIC phenomenon. Although the emission fluorescence of SiO$_2$/Pt/Ti/Si wafers was higher than that of SiO$_2$/Si wafers, the lower chemical stability of these wafers precluded their use for further studies. Therefore, hAChE immobilization was performed on uncoated silicon wafers, for which high stability was coupled with acceptable fluorescence emission intensity.

Measurements with CLSM, AFM and SAM all supported the conclusion that hAChE was mostly confined to the top of SiO$_2$ structures. This confinement might be because of chemical contrast which resulted from either the structuring of the wafer or the cleaning procedures used before derivatisation. A batch-wise activity assay confirmed that the immobilized enzyme was active. Finally, propidium was shown to selectively label the immobilised hAChE without any interaction with enzyme-free silicon or metal surfaces.

References

1. Rusmini F, Zhong Z, Feijen J (2007) Protein immobilization strategies for protein biochips. Biomacromolecules 8(6):1775–1789
2. Ansari SA, Husain Q (2012) Potential applications of enzymes immobilized on/in nano materials: A review. Biotechnol Adv 30 (3):512–523
3. International AsD (2009) World Alzheimer Report 2009 - Executive Summary. http://www.alz.co.uk/research/world-report
4. Birks J (2006) Cholinesterase inhibitors for Alzheimer's disease. Cochrane Database Syst Rev (1):CD005593
5. Inestrosa NC, Alvarez A, Perez CA, Moreno RD, Vicente M, Linker C, Casanueva OI, Soto C, Garrido J (1996) Acetylcholinesterase accelerates assembly of amyloid-beta-peptides into Alzheimer's fibrils: possible role of the peripheral site of the enzyme. Neuron 16(4):881–891
6. Alvarez A, Opazo C, Alarcon R, Garrido J, Inestrosa NC (1997) Acetylcholinesterase promotes the aggregation of amyloid-beta-peptide fragments by forming a complex with the growing fibrils. J Mol Biol 272(3):348–361
7. Bartolini M, Bertucci C, Cavrini V, Andrisano V (2003) beta-Amyloid aggregation induced by human acetylcholinesterase: inhibition studies. Biochem Pharmacol 65(3):407–416
8. Bolognesi ML, Matera R, Minarini A, Rosini M, Melchiorre C (2009) Alzheimer's disease: new approaches to drug discovery. Curr Opin Chem Biol 13(3):303–308
9. Forsberg EM, Green JR, Brennan JD (2011) Continuous flow immobilized enzyme reactor–tandem mass spectrometry for screening of AChE inhibitors in complex mixtures. Anal Chem 83(13):5230–5236

10. da Silva JI, de Moraes MC, Vieira LC, Correa AG, Cass QB, Cardoso CL (2012) Acetylcholinesterase capillary enzyme reactor for screening and characterization of selective inhibitors. J Pharm Biomed Anal. in press. doi:10.1016/j.jpba.2012.01.026

11. Bartolini M, Cavrini V, Andrisano V (2005) Choosing the right chromatographic support in making a new acetylcholinesterase-micro-immobilised enzyme reactor for drug discovery. J Chromatogr A 1065(1):135–144

12. Bartolini M, Cavrini V, Andrisano V (2004) Monolithic micro-immobilized-enzyme reactor with human recombinant acetylcholinesterase for on-line inhibition studies. J Chromatogr A 1031(1–2):27–34

13. Bartolini M, Cavrini V, Andrisano V (2007) Characterization of reversible and pseudo-irreversible acetylcholinesterase inhibitors by means of an immobilized enzyme reactor. J Chromatogr A 1144(1):102–110

14. Kao FS, Ger W, Pan YR, Yu HC, Hsu RQ, Chen HM (2012) Chip-based protein-protein interaction studied by atomic force microscopy. Biotechnol Bioeng. doi:10.1002/bit.24521

15. Groves JT, Parthasarathy R, Forstner MB (2008) Fluorescence imaging of membrane dynamics. Annu Rev Biomed Eng 10:311–338

16. Lambacher A, Fromherz P (1996) Fluorescence interference-contrast microscopy on oxidized silicon using a monomolecular dye layer. Appl Phys A Mater Sci Process 63(3):207–216

17. Han Y, Mayer D, Offenhausser A, Ingebrandt S (2006) Surface activation of thin silicon oxides by wet cleaning and silanization. Thin Solid Films 510:175–180

18. Ellman GL, Courtney KD, Andres V Jr, Feather-Stone RM (1961) A new and rapid colorimetric determination of acetylcholinesterase activity. Biochem Pharmacol 7:88–95

19. Ajo-Franklin CM, Yoshina-Ishii C, Boxer SG (2005) Probing the structure of supported membranes and tethered oligonucleotides by fluorescence interference contrast microscopy. Langmuir 21 (11):4976–4983

20. Bourne Y, Taylor P, Radic Z, Marchot P (2003) Structural insights into ligand interactions at the acetylcholinesterase peripheral anionic site. EMBO J 22(1):1–12

21. Haynes WM, Lide DR (2010) Handbook of chemistry and physics, 91st edn. CRC Press, Boca Raton

22. van Delft FCMJM, Nieuwenhuys BE (1985) Correlation of Nucleation and Growth Modes with Wetting, Alloy Segregation, Catalyst Preparation and Strong-Metal Support Interaction. Solid State Ionics 16(1–4):233–240

23. Taylor P, Lappi S (1975) Interaction of fluorescence probes with acetylcholinesterase. The site and specificity of propidium binding. Biochemistry 14(9):1989–1997

24. Taylor P, Lwebuga-Mukasa J, Lappi S, Rademacher J (1974) Propidium—a Fluorescence Probe for a Peripheral Anionic Site on Acetylcholinesterase. Mol Pharmacol 10(4):703–708

25. Godoy S, Violot S, Boullanger P, Bouchu MN, Leca-Bouvier BD, Blum LJ, Girard-Egrot AP (2005) Kinetics study of Bungarus fasciatus venom acetylcholinesterase immobilised on a Langmuir–Blodgett proteo-glycolipidic bilayer. Chembiochem 6(2):395–404

26. Zheng Z, Zhou Y, Li X, Liu S, Tang Z (2011) Highly-sensitive organophosphorous pesticide biosensors based on nanostructured films of acetylcholinesterase and CdTe quantum dots. Biosens Bioelectron 26(6):3081–3085

27. Zhang X, Guo Q, Cui D (2009) Recent advances in nanotechnology applied to biosensors. Sensors (Basel) 9(2):1033–1053

28. Bartolini M, Cavrini V, Andrisano V (2005) Batchwise covalent immobilization of human acetylcholinesterase: kinetic and inhibition spectrophotometric studies. Anal Biochem 342(1):163–166